BIOCHEMISTRY
including biophysical chemistry & molecular biology
Article

Biochemistry **2010,** *49,* 7459–7466 7459
DOI: 10.1021/bi1008134

Creation and Biophysical Characterization of a High-Affinity, Monomeric EGF Receptor Ectodomain Using Fluorescent Proteins†

Noga Kozer,[‡,§,⊥] Christine Henderson,[‡,§,⊥] Michael F. Bailey,[∥] Julie Rothacker,[‡] Edouard C. Nice,[‡] Anthony W. Burgess,[‡] and Andrew H. A. Clayton*[,‡,§]

[‡]*Ludwig Institute for Cancer Research, P.O. Box 2008, Royal Melbourne Hospital, Victoria 3050, Australia,* [§]*Centre for Microphotonics, Faculty of Engineering and Industrial Sciences, Swinburne University of Technology, P.O. Box 218, Hawthorn, Victoria 3122, Australia, and* [∥]*Department of Biochemistry and Molecular Biology, BIO21 Institute, The University of Melbourne, Melbourne, Victoria 3050, Australia.*
[⊥]*These authors contributed equally to this work.*

Received May 21, 2010; Revised Manuscript Received August 2, 2010

ABSTRACT: X-ray structural studies revealed two conformations of the epidermal growth factor receptor (EGFR) ectodomain (ECD): a compact, tethered conformation in the absence of EGF and an untethered or extended conformation in the presence of EGF. An EGFR-ECD derivative with a monomeric red fluorescent protein (mRFP) at the N-terminus and an enhanced green fluorescent protein (eGFP) at the C-terminus (dual-tag-EGFR-ECD) was created and characterized. The dual-tag-EGFR-ECD construct was shown to have high affinity (nanomolar range) for both EGF and EGFR monoclonal antibody (mAb528). The dual-tag-EGFR-ECD was further characterized by fluorescence-detected analytical ultracentrifugation, lifetime FRET, and fluorescence anisotropy. We found no evidence of a tethered unliganded conformation, nor did we observe a large shape change upon ligand binding as predicted by the crystal models. Increases in steady-state anisotropy upon binding of EGF to the dual-tag-EGFR-ECD were observed and interpreted as changes in the protein flexibility and dynamics. We conclude the fluorescent protein tags perturb the EGFR-ECD structure, making it extended with a 50-fold higher affinity for EGF relative to that of the nontagged EGFR-ECD.

The EGFR[1] plays an important role in development, homeostasis, and diseases such as cancer (*1*). Activation of the EGFR tyrosine kinase is believed to occur via a ligand-induced dimerization (*2*), ligand-induced conformational change within a preformed dimer (*3*), and/or oligomerization (*4*, *5*). The extracellular domain (ECD) of EGFR contains two ligand binding domains (domains I and III) and two cystine-rich domains (domains II and IV) (*1*). EGFR has two conformations in the crystal: a tethered conformation and an untethered or extended one. In the unliganded state of the EGFR-ECD, the monomeric receptor exists in the tethered intramolecular conformation in which a dimerization motif is prevented from mediating receptor−receptor interaction by a "tether" between domains II and IV (*6*). The liganded EGFR-ECD exists in the untethered conformation in which the domain II−IV tether is released and a dimerization arm is exposed ready to oligomerize with itself, erbB2, or the other three liganded ErbB members (*6*). Ligand-induced conformational changes in the EGFR-ECD have been inferred by tryptophan fluorescence spectroscopy (*7*) and X-ray scattering in solution (*8*). More recently, a crystal structure of the *Drosophila* analogue of the EGFR-ECD showed an unliganded and untethered structure (*9*), but the relevance of this structure to the human EGFR-ECD is not known. An outstanding question raised by these studies of the EGFR-ECD is to what extent distinct tethered, untethered, or possibly intermediate states are populated in solution.

In an attempt to answer this question, we designed, expressed, purified, and characterized an EGFR-ECD construct doubly tagged with mRFP at the N-terminus and eGFP at the C-terminus (dual-tag-EGFR-ECD). This design was based on the crystal structures that predict a large change in the separation of the EGFR-ECD termini in the tethered and untethered states. As shown in Figure 1, models of the EGFR-ECD, with probes attached, reveal a large difference in the separation of the tags between tethered [4.5 nm (Figure 1A)] and untethered [10.8 nm (Figure 1B)] conformations. These conformational differences should be detectable with biophysical methods such as analytical ultracentrifugation, fluorescence polarization, and Forster resonance energy transfer (FRET). In what follows, we present a biochemical and biophysical characterization of this construct using conformation-sensitive fluorescence techniques and relate the data to the conformation(s) of the EGFR-ECD.

EXPERIMENTAL PROCEDURES

Structural Model of the Dual-Tag-EGFR-ECD. Fusion constructs containing the three components of the designed protein dual-tag-EGFR-ECD (EGFR-ECD, eGFP, and mRFP)

†A.H.A.C. was partially supported by an R. D. Wright Biomedical Career Development Award from the Australian National Health and Medical Research Council (NHMRC). This work was also supported by NHMRC Project Grants 280918 and 433624 and NHMRC Program 280912.

*To whom correspondence should be addressed: Centre for Microphotonics, Swinburne University of Technology, P.O. Box 218, Hawthorn, Victoria 3122, Australia. Telephone: +61-392145719. Fax: +61-392145435. E-mail: aclayton@swin.edu.au.

[1]Abbreviations: EGF, epidermal growth factor; EGFR, EGF receptor; mRFP, monomeric red fluorescent protein; eGFP, enhanced green fluorescent protein; dual-tag-EGFR-ECD, EGFR ectodaomain labeled with mRFP and eGFP; FRET, Forster resonance energy transfer; PDB, Protein Data Bank.

Published on Web 08/17/2010

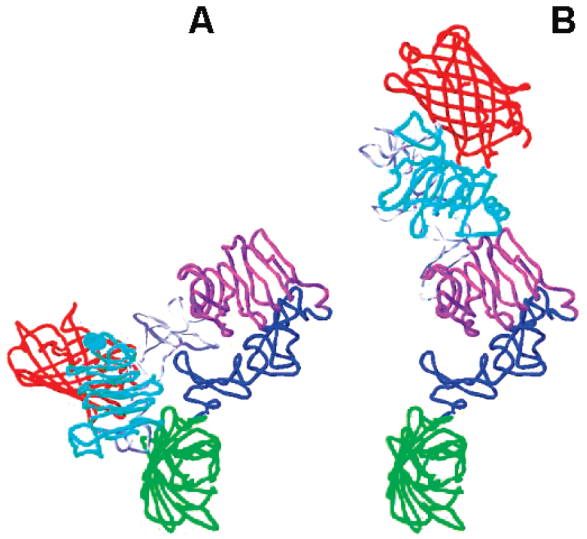

FIGURE 1: Models of the dual-tag-EGFR-ECD. EGFR-ECD fused to mRFP at the N-terminus (red ribbon) and eGFP at the C-terminus (green ribbon) in the tethered (A) and untethered (B) conformations. The EGFR-E-CD is color-coded: aqua, purple, magenta, and blue fore domains I−IV, respectively. Note the large change in separation between the eGFP and mRFP in the EGF-bound receptor [10.8 ± 4 nm (B)] as compared to the free one [4.5 ± 2 nm (A)].

were generated in silico using the script described by Pham et al. (*10*). These were used to explore the possible spacing between the fluorescent proteins (eGFP as the donor and mRFP as the acceptor) and calculate an averaged donor−acceptor distance for the tethered and untethered conformations. For the tethered unliganded EGFR-ECD, we used the coordinates of PDB entry 1NQL (*6*). For the untethered liganded EGFR-ECD, we used the model suggested by Burgess et al. based on PDB entry 1IVO (*11*, *12*). A single PDB entry (1S6Z, eGFP) was used for both fluorescent proteins in the model as the overall structures of eGFP and mRFP are very similar and the models were used for rough distance estimation and not for evaluation of fine details. The models (Figure 1A,B) were subjected to rigid-body rotation conformations of the fluorescent proteins relative to the EGFR-ECD using the computational tool FPMOD (*10*). A set of 10 models was generated for each conformation, from which an average eGFP−mRFP separation (measured from the chromophore centers) was calculated to be 4.5 ± 2 nm for the tethered state and 10.8 ± 4 nm for the untethered state.

Plasmids. The dual-tag-EGFR-ECD plasmid was generated in three steps: (1) amplification of the EGFR-ECD from the full-length receptor sequence (first 621 N-terminal amino acids), (2) cloning eGFP C-terminal to the EGFR-ECD to create EGFR-ECD-eGFP, and (3) cloning mRFP N-terminal to the EGFR-ECD-eGFP to create mRFP-EGFR-ECD-eGFP (dual-tag-EGFR-ECD). The complete construct contained 3.2 kb that translates into a 1085-amino acid protein with an estimated molecular mass of 123 kDa. A detailed description of how the plasmid was made is included in the Supporting Information.

Cell Culture and DNA Transfection. Transient transfection of plasmids into human 293T cells (maintained in DMEM supplemented with 10% FCS) was conducted to establish protein expression. Cells (2×10^5) were transfected with 1 μg of plasmid DNA using FuGENE (Roche Molecular Biochemicals, Sydney, Australia) according to the manufacturer's instructions. Supernatants and cells were harvested 48 h after transfection. Cells were lysed in 500 μL of lysis buffer [1% Triton X-100, 10% glycerol, 150 mM NaCl, 50 mM HEPES (pH 7.4), 1 mM EGTA, and complete protease inhibitor mixture (Roche Molecular Biochemicals)]. Aliquots of supernatant and lysate were immunoprecipitated with EGFR monoclonal antibody (mAb528)-coated beads (G Sepharose 4 fast Flow beads, Amersham) before samples were subjected to Western blot analysis. A stable transfection of the DNA was conducted in Hek293 cells as described above. Positive clones were selected using 1.5 mg/mL neomycin (G418) (Cellgro) exposure over 4 weeks. Isolated colonies were trypsinized and further diluted in 96-well plates. Stable cell lines were scaled up from the 96-well plates as they became confluent. Clones were selected for protein expression according to their fluorescence under the microscope and by the protein expression of the supernatant as assessed by Western blotting.

Western Blot Analysis. Products of the immunoprecipitations, cell lysate, and supernatant were mixed with SDS sample buffer containing 1.5% β-mercaptoethanol. Samples were run on 4 to 12% NuPAGE Bis-Tris polyacrylamide gels (Invitrogen) and transferred to nitrocellulose membranes (Protran, Whatman). Membranes were probed with a primary anti-EGFR antibody, mAb806 (*13*), and a secondary antibody of goat anti-mouse IRDye 800CW (LI-COR). Membranes were scanned using the Odyssey Infrared Imaging system (LI-COR Biotechnology).

Protein Purification. Stably transfected HEK293 cells (human embryonic kidney) expressing the dual-tag-EGFR-ECD (or the singly labeled EGFR-ECD constructs) were grown in 15 cm tissue culture dishes for 5 days until the cells were confluent. The supernatent was collected, spun at 450*g* for 30 min, and filtered (Fast PES Filter Unit 0.2 μM, Nalgene filtration products) to generate a batch of conditioned media for protein purification. Protein was purified using a mAb528 affinity column (details below). Positive fractions were concentrated using Vivaspin2, 5000 MWCO PES (VivaScience, Sartorius) and further purified by size exclusion chromatography (Superose 12 3.2/30, Amersham Biosciences). Positive homogeneous dual-tag-EGFR-ECD fractions (as determined by SDS−PAGE) were pooled and stored at 4 °C for further analysis.

mAb528 Affinity Column. The dual-tag-EGFR-ECD (or the singly labeled EGFR-ECD constructs) was purified with an affinity column as previously described (*19*) with some minor adjustments. NHS-activated Sepharose beads (GE Healthcare Life Sciences) were washed with ice-cold HCl (1 mM) to remove excess 2-propanol and equilibrated with carbonate buffer (pH 8.3). Anti-EGFR antibody mAb528 was diluted in the same buffer (2 mg/mL), added to the beads (1 mg of mAb528/mL of suspended beads), and incubated overnight at 4 °C while being rotated. mAb528-bound beads were resuspended in 1 M ethanolamine at room temperature for 2 h and washed with HT-PBS until the pH was restored before the column was packed. Conditioned medium was injected into the column at a rate of 1 mL/min in 500 mL batches. The column was washed with PBS, and elution was conducted using 0.1 M glycine (pH 3) directly into 1 M Tris-HCl (pH 8.0) to neutralize the eluate.

Protein Characterization. Fractions purified by the two-step procedure (mAb528 affinity and size exclusion columns) were analyzed by SDS−PAGE (4 to 12% Bis-Tris gel, Invitrogen) and either Coomassie or silver stained to ensure homogeneity of fractions. Most purified fractions were pooled and characterized by mass spectrometry. The bands were excised from a Coomassie-stained gel, and mass spectrometry (Maldi-QStar/MS/MS) was performed by the JPSF Ludwig Institute for Cancer Research which confirmed the size and purity of the protein.

UV−vis absorption scans of the protein showed the characteristic absorption at 280, 488, or 580 nm. Protein concentrations were determined by 280 nm absorbance using a molecular mass of 123 kDa and an extinction coefficient of 101000 M^{-1} cm^{-1} for the dual-tag-EGFR-ECD [Expasy ProtParam Tool (*14*)]. Emission spectra typical of eGFP and mRFP were recorded on a commercial spectrofluorimeter (Varian Cary eclipse, Melbourne, Australia).

Binding Analysis. Interaction analyses were monitored in real time on an instrumental optical biosensor using surface plasmon resonance detection (Biacore 3000, BIAcore, GE Heatlhcare, Uppsala, Sweden). hEGF (ProSpecBio) or mAb528 was immobilized onto the CM5 biosensor surface using amine coupling chemistry (*N*-hydroxysuccinimide and *N*-ethyl-*N*′-dimethylaminopropylcarbodiimide) at a flow rate of 20 μL/min. Immobilization levels were 90 response units (RU), equivalent to 0.9 ng of hEGF/mm^2, or 2000 RU, equivalent to 0.9 ng of mAb528/mm^2 on the sensor chip. The dual-tag-EGFR-ECD was diluted in Biacore buffer (HBS) [10 mM Hepes (pH 7.4) containing 3.4 mM EDTA, 0.15 mM NaCl, and 0.005% (v/v) Tween 20] to the appropriate concentration. Samples (140 μL) at concentrations of 4.9−600 nM were injected sequentially over the sensor surfaces at a flow rate of 100 μL/min. Following completion of the injection phase, dissociation was monitored in Biacore buffer at the same flow rate for 3600 s. The sensor surface and sample blocks were maintained at 25 °C. The sensor surface was regenerated between injections, using 30 μL of 10 mM glycine-HCl (pH 2.0). This treatment did not denature hEGF or mAb528 immobilized onto the sensor surface, as shown by equivalent signals upon reinjection of the receptor.

Fluorescence-Detected Analytical Ultracentrifugation. The oligomeric state of the dual-tag-EGFR-ECD was determined by analytical ultracentrifugation. Sedimentation velocity experiments were conducted in an Optima XL-A analytical ultracentrifuge (Beckman-Coulter) equipped with a Fluorescence Detection System (FDS) using an An-Ti60 rotor and double-sector 12 mm path length cells containing sapphire windows and charcoal-filled Epon centerpieces. Samples of 300 μL comprising 200 nM dual-tag-EGFR-ECD alone or in the presence of 200 nM EGF were centrifuged at 50000 rpm and 20 °C in the experimental buffer (PBS). Radial fluorescence scans (excitation at 488 nm, emission at > 520 nm) were collected continuously from 5.8 to 7.3 cm using five averages and a radial resolution of 20 μm. Data were analyzed in terms of a continuous mass distribution model using SEDFIT (*15*). For the purpose of the analysis, $\bar{\nu}$, ρ, and η were assigned values of 0.73 mL/g, 1.000 g/mL, and 1.002×10^{-2} P [SEDENTERP (*16*)]. During the analysis, TI and RI noise were removed and the frictional ratio was freely optimized for the best fit (that is, f/f_0 was determined as part of the analysis).

Multifrequency Lifetime-Based FRET Measurements and Analysis. Multifrequency fluorescence lifetime imaging microscopy (LIFA, Lambert instruments, Leutingivolde, The Netherlands) was used to determine the eGFP lifetime. The setup has been described previously (*17*). FRET efficiencies between the N- and C-terminal probes in the dual-tag-EGFR-ECD were calculated from the measured lifetimes. The phase and modulation of the detected fluorescence were recorded at five optical modulation frequencies (10, 20, 30, 40, and 70 MHz) using software provided by the manufacturer, and the data were fit to a single lifetime component (LIFA software).

Fluorescence Anisotropy Measurements. The rotational dynamics of proteins in aqueous solution were obtained from steady-state fluorescence anisotropy measurements, conducted on a commercial spectrofluorimeter (Varian Cary eclipse) equipped with polarizers, and a thermostated bath, which allowed the sample temperature to be maintained at 25 ± 0.2 °C. Anisotropy was measured for the dual-tag-EGFR-ECD (40 nM) in the presence or absence of excess mEGF (10 μM). The EGF-induced increase in light scattering, which might affect *r* values, was excluded by performing a control experiment in the absence of fluorescent protein. Each measurement was repeated at least five times and averaged. The apparent rotational correlation time, ϕ_{app}, was calculated from the fluorescence anisotropy using the Perrin equation:

$$r = \frac{r_0}{1 + \frac{\tau}{\phi_{app}}} \quad (1)$$

where τ is the fluorescence lifetime, r is the measured anisotropy, and r_0 is the limiting anisotropy. The excitation and emission wavelengths used are 470 and 509 nm for eGFP and 584 and 608 nm for mRFP, respectively. The r_0 values of 621-eGFP (0.389 ± 0.002) and mRFP-621 (0.400 ± 0.01) were measured in a ~100% glycerol solution at 20 °C. The fluorescence lifetimes used are 2.8 and 3.0 ns for eGFP and mRFP, respectively.

RESULTS AND DISCUSSION

Protein Characterization and EGF Binding. The dual-tag-EGFR-ECD was cloned into a pEGFP-N1 plasmid to include the 621 amino acids of the EGFR-ECD flanked by mRFP (225 amino acids) at the N-terminus and eGFP (239 amino acids) at the C-terminus. The complete cDNA sequence contains 3.2 kb and translates into a 123 kDa protein. The plasmid was transfected into Hek293 cells, and the protein was translated and secreted into the tissue culture medium due to a signal peptide upstream of mRFP. A two-step procedure was used to purify the protein: affinity column with EGFR antibodies (mAb528) followed by size exclusion chromatography. The size of the dual-tag-EGFR-ECD was confirmed to be 140−150 kDa by SDS−PAGE [Figure 2, top panel; the slightly higher molecular mass is due to protein glycosylation (data not shown)], and typical eGFP and mRFP excitation and emission spectra were routinely recorded in a fluorometer before each lifetime and anisotropy experiment to verify probe stability (Figure 2, bottom panel). Biacore analysis was used to determine if the dual-tag-EGFR-ECD exhibits high-affinity binding to both its ligand (EGF; K_D = 6 nM) and a monoclonal EGFR antibody (mAb528; K_D = 14 nM) (Figure 3). For comparison, the binding affinity of the unlabeled EGFR-ECD was found to be ~300 nM for EGF (*8*, *18*, *19*) and 19 nM for mAb528 (data not shown). Interestingly, the dual-tag-EGFR-ECD affinity for its ligand (6 nM) is almost 2 orders of magnitude higher than that of the unlabeled EGFR-ECD (300 nM). In fact, the high affinity value recorded for the dual-tag-EGFR-ECD in solution resembles more the K_D value measured for the majority of full-length EGF receptors on the cell surface [1−2 nM (*20*)]. It is worth noting that the increased affinity originates from the 30−50-fold decrease in the dissociation constant, while the association constant seems unchanged. Two lines of evidence argue against the possibility that the high affinity of the dual-tag-EGFR-ECD for EGF is a result of serendipitous interactions between EGF and one or both of the protein tags. First, it has been shown that the EGF-induced phosphorylation of the full-length receptor proteins, with FP fused to the ECD region, is indistinguishable from that of the native proteins (*21*). This is strong evidence that

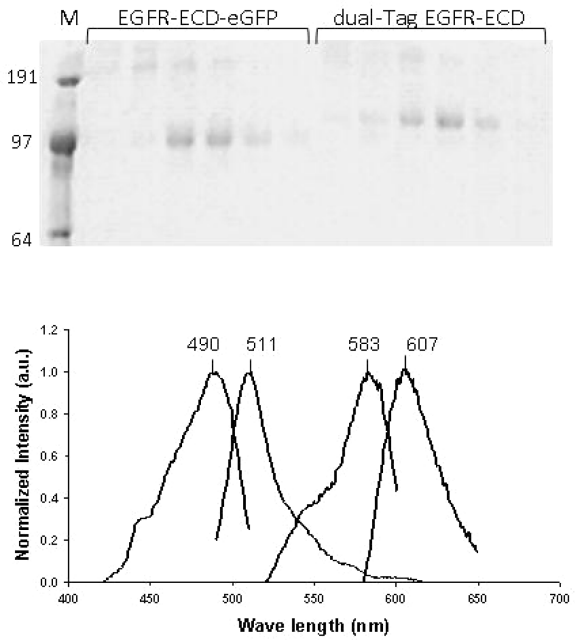

FIGURE 2: Protein characterization. Coomassie-stained SDS−PAGE analysis of the singly and doubly labeled EGFR-ECD glycosylated proteins (EGFR-ECD-eGFP and dual-tag-EGFR-ECD, respectively) reveals the expected molecular mass of ~110 kDa for EGFR-ECD-eGFP and ~150 kDa for the dual-tag-EGFR-ECD (top). Fluorescence excitation and emission spectra of the dual-tag-EGFR-ECD (bottom). The two left spectra represent excitation and emission of eGFP attached to the EGFR-ECD (490 and 511 nm, respectively). The two right spectra represent excitation and emission of mRFP attached to the EGFR-ECD (583 and 607 nm, respectively).

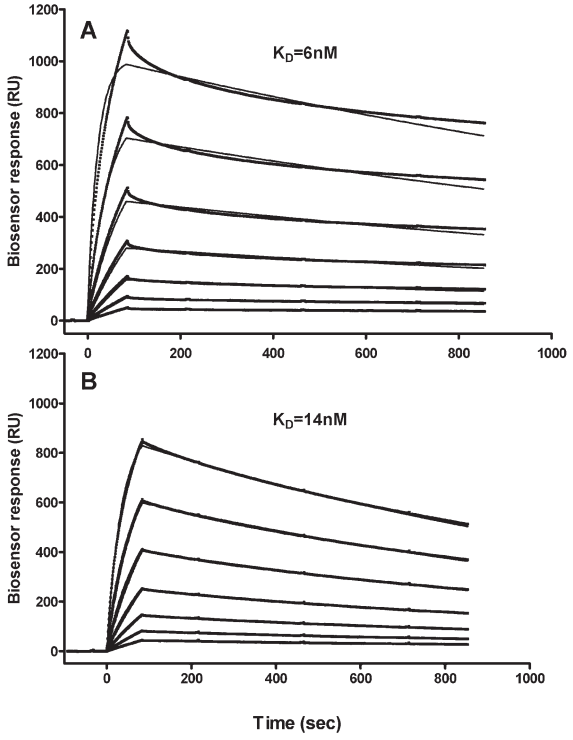

FIGURE 3: Biacore analysis of the interactions between the dual-tag-EGFR-ECD with immobilized EGF or EGFR monoclonal antibody (mAb) 528. (A) Interaction of the dual-tag-EGFR-ECD with an immobilized EGF surface. Data points of increasing amplitudes correspond to sensorgrams obtained with increasing dual-tag-EGFR-ECD concentrations (9.4, 18.8, 37.5, 75, 150, and 300 nM). Fine lines are fits to a 1:1 Langmuir binding model, yielding a K_D value of 6 nM. (B) Interaction of the dual-tag-EGFR-ECD (concentration as in panel A) with the immobilized mAb528 surface. Fine lines are fits to a 1:1 Langmuir binding model, yielding a K_D value of 14 nM.

EGF binds its proper binding site in chimeric receptors expressed on the cell surface. Second, we have Biacore data to support the ability of EGF to compete with the dual-tag-EGFR-ECD on binding surface-immobilized mAb528 (data not shown). Antibody mAb528 binds to domain II, competing for the major ligand contact surface. On the basis of protein size, its fluorescent spectra, and high-affinity binding to EGF and mAb528, we conclude that the dual-tag-EGFR-ECD is correctly folded, active, and therefore suitable for reporting conformational changes upon EGF binding. The significantly higher affinity of the dual-tag-EGFR-ECD for EGF compared to the unlabeled EGFR-ECD implies that there might be a structural difference between the two. To examine the conformations of the dual-tag-EGFR-ECD in solution, we have measured its oligomeric state, rotational dynamics, and conformations in the liganded and unliganded states using a number of fluorescence techniques.

Fluorescence-Detected Analytical Ultracentrifugation. Fluorescence-detected analytical ultracentrifugation [AUC (*22*)] together with size distribution analysis (*15*) was used to characterize the oligomeric states and overall shape of the dual-tag-EGFR-ECD in the presence and absence of EGF. Figure 4A presents a series of radial fluorescence scans of a 200 nM sample of the dual-tag-EGFR-ECD recorded at various times during centrifugation (increasing from left to right). For the sake of clarity, every fifth scan is shown. The solid lines were obtained from a $c(M)$ analysis (*15*), the distribution for which is shown in Figure 4C. The distribution is monomodal, indicating that the sample sediments as a single species. The maximum of the distribution corresponds to a modal molar mass of 146 kDa. This is in good agreement with the theoretical figure of 123 kDa predicted from the amino acid sequence of the construct and the SDS−PAGE analysis (Figure 2A). The dual-tag-EGFR-ECD construct was then centrifuged as described above, but in the presence of a molar equivalent of EGF (Figure 4D). In this case, the distribution was also essentially monomodal (Figure 4F); however, the modal molar mass was increased by 8 kDa to 154 kDa, consistent with the binding of EGF (calculated molecular mass of 6.5 kDa).

The similarity between the frictional ratios recovered for the dual-tag-EGFR-ECD alone (1.52) and in the presence of EGF (1.57) indicates that in both the free and EGF-bound forms the dual-tag-EGFR-ECD adopts a similar conformation. The fact that these figures are both greater than 1.2 provides evidence that the receptor does not adopt a globular structure, but rather a somewhat elongated one. The small change in friction ratio that accompanies ligand binding is not in accord with the large shape change predicted by the models (Figure 1). No dimeric species could be detected at these concentrations from the molecular mass distribution analysis. The analytical centrifugation data therefore indicate that on average there is no significant change in the overall dual-tag-EGFR-ECD shape upon ligand binding.

Lifetime FRET Measurements. To investigate the conformational states more directly, multifrequency, lifetime-based FRET was used to measure distances between the N- and C-terminal tags in a solution of 200 nM dual-tag-EGFR-ECD in the presence or absence of excess EGF. In this approach, FRET from the eGFP donor to the mRFP acceptor is detected by a decrease in the fluorescence lifetime of the eGFP fluorophore (*23*). To estimate FRET efficiency, data from five frequencies (10−70 MHz) were fit to a single-lifetime model (Figure 5A). As one can see from a

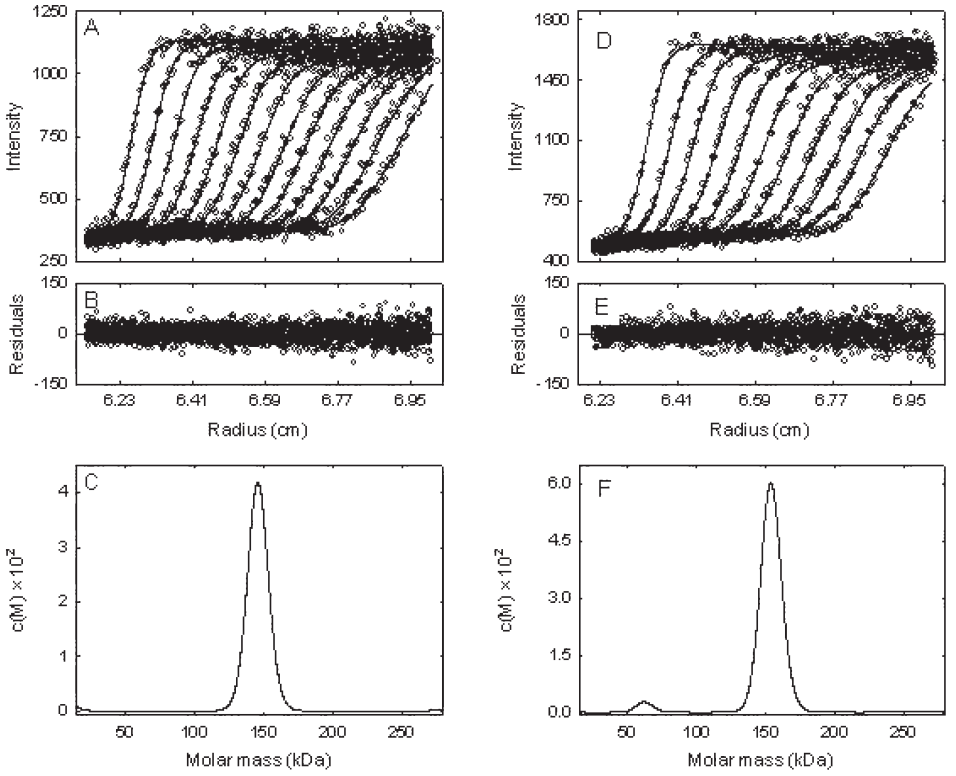

FIGURE 4: Fluorescence-detected analytical ultracentrifugation (AUC) analysis of the free and EGF-bound dual-tag-EGFR-ECD. Sedimentation velocity data and analysis of the free (left panels) and EGF-bound (right panels) dual-tag-EGFR-ECD. (A and D) Distributions of the intensity of fluorescence vs radius at different times (circles for data points and lines for fits). (B and E) Plots of the residuals between experimental data and the fits. (C and F) Fitted molar mass distributions. The molecular mass for the dual-tag-EGFR-ECD is 146 kDa (C) and for the dual-tag-EGFR-ECD in complex with EGF 154 kDa (F).

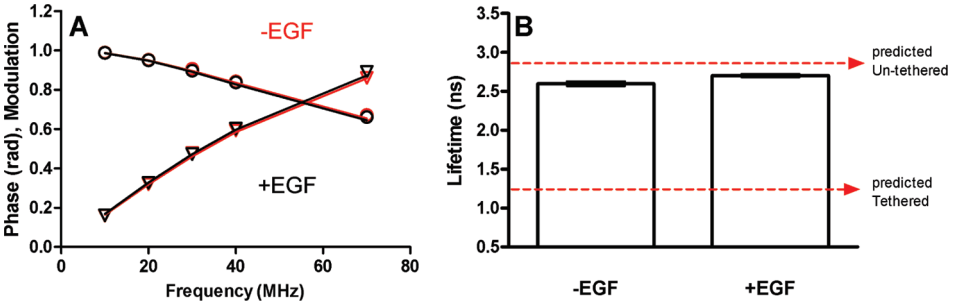

FIGURE 5: Multifrequency lifetime-based FRET measurements of the free and EGF-bound dual-tag-EGFR-ECD. The lifetime of dual-tag-EGFR-ECD samples with or without excess EGF in solution was measured using multiple frequencies (10−70 MHz). (A) The phase (triangles) and modulation (circles) of the fluorescence are plotted as a function of modulation frequency. Lines represent the fits to a single lifetime component. (B) Effect of EGF on the lifetime of the eGFP tag of the dual-tag-EGFR-ECD: (left) lifetime in the absence of EGF (2.6 ns) and (right) lifetime in the presence of EGF (2.7 ns). The top and bottom dashed lines (2.83 and 1.24 ns) represent the theoretical lifetimes predicted for the untethered and tethered conformations, respectively. Theoretical lifetime values were calculated on the basis of the distances between the probes in the dual-tag-EGFR-ECD model (Figure 1). See the text for details.

comparison of data and fits, the single-lifetime model provided an adequate description of the data. The donor-only eGFP lifetime measured for the singly labeled EGFR-ECD (EGFR-ECD-eGFP) was 2.85 ± 0.03 ns in the presence or absence of EGF. In the dual-tag-EGFR-ECD, a decrease in the eGFP lifetime was observed from 2.85 ± 0.03 to 2.6 ± 0.02 ns which indicates FRET between the eGFP and mRFP with an average efficiency of ~9% (Figure 5B). In the dual-tag-EGFR-ECD−EGF complex, the average lifetime of the eGFP increased only slightly (2.7 ± 0.02 ns) relative to that of the EGF-free receptor, indicating a small decrease in energy transfer efficiency to 5% and therefore a small increase in the average distance between the probes (Figure 5B). Because the change in transfer efficiency is only 4%, we suggest there is a negligible change in distance between the probes upon ligand binding. We also considered alternative explanations for the FRET observations. The low measured FRET efficiency and small differences in measured efficiencies could in principle be due to donors with no attached, or poorly matured, acceptors. However, these possibilities are excluded by the AUC, SDS−PAGE data and the fluorescence spectroscopy measurements that showed the protein contains an attached, mature RFP chromophore. Another possible cause for the low efficiency could be a small orientation factor (κ^2) for the probes. For this to occur, the probe dipoles would have to be fixed in a nearly orthogonal arrangement. This is unlikely from inspection of the model in Figure 1 and from our anisotropy measurements, which indicate substantial local probe motions. Assuming a Forster distance of 4.7 nm for the eGFP−mRFP donor−acceptor pair (*23*), the lifetimes

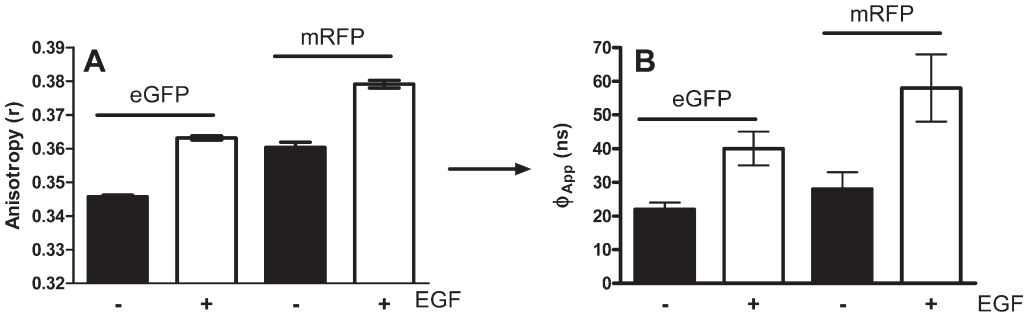

FIGURE 6: Rotational dynamics of eGFP and mRFP probes in the free or EGF-bound dual-Tag-EGFR-ECD. (A) Steady-state fluorescence anisotropy (r) of the dual-tag-EGFR-ECD eGFP tag (left two columns) and mRFP tag (right two columns) in the absence (black bars) and presence (white bars) of EGF. The data presented are averages ± standard error from five independent measurements. (B) Apparent rotational correlation time, ϕ_{app}, of the dual-tag-EGFR-ECD eGFP tag (left two columns) and mRFP tag (right two columns) in the absence (black bars) and presence (white bars) of EGF. ϕ_{app} was calculated from the fluorescence anisotropy in panel A using the Perrin equation (see Experimental Procedures).

predicted from the dual-tag-EGFR-ECD model are 2.83 and 1.24 ns for the untethered conformation (Figure 1B, donor−acceptor distance of 10.8 nm, FRET efficiency of < 1%) and tethered conformation (Figure 1A, donor−acceptor distance of 4.5 nm, FRET efficiency of > 50%), respectively. These calculated values are presented for reference as dotted lines in Figure 5B. It is very clear that the lifetime values measured for the dual-tag-EGFR-ECD do not support a highly populated tethered conformation in the absence of ligand. Moreover, these results are in contrast with the predicted change in separation between the N- and C-termini expected for a tethered to untethered transition.

Taken together, the two sets of data (AUC and lifetime FRET analysis) imply that (a) there is no large change in the structure or overall shape of the dual-tag-EGFR-ECD upon ligand binding and (b) the more abundant conformation for the dual-tag-EGFR-ECD, whether free or bound to EGF, is the untethered rather than the tethered one.

Steady-State Anisotropy. A change in the dual-tag-EGFR-ECD shape and/or dynamics upon ligand binding can be also detected by measuring its steady-state anisotropy. The rotational dynamics of the eGFP and mRFP probes fused to the C- and N-termini of the EGFR-ECD (40 nM dual-tag-EGFR-ECD) were measured using fluorescence polarization anisotropy (*24*). The raw anisotropy values (r) are presented in Figure 6A. Both probes demonstrated an increase of ~5% in r values upon EGF binding. The dynamical range of the measured anisotropies is typically not large (0.3−0.4) for eGFP or mRFP because of the size of the probes. Nevertheless, the change in anisotropy between the free and EGF-bound dual-tag-EGFR-ECD was found to be statistically significant ($p < 0.001$) and represents a 16% change versus that expected from the probes free in solution to completely immobile (the full range represents a 30% change in anisotropy). To gain a better appreciation of the dynamical changes involved, the anisotropy data were converted to apparent correlation times. The apparent rotational correlation times, ϕ_{app}, are presented in Figure 6B. ϕ_{app} values were calculated from the r value presented in Figure 6A using the Perrin equation (eq 1). As r_0 is a critical parameter in calculating ϕ_{app}, we measured very carefully r_0 values of the singly labeled EGFR-ECD in an ~100% glycerol solution at 20 °C. The EGFR-ECD-eGFP r_0 was found to be 0.389 ± 0.002, and the mRFP-EGFR-ECD yielded an r_0 of 0.400 ± 0.01. The fluorescence lifetimes (τ) used were 2.8 and 3.0 ns for eGFP and mRFP, respectively. Figure 6B shows that in the absence of EGF the ϕ_{app} of the eGFP tag at the C-terminus was calculated to be 22 ± 2 ns and increased to 40 ± 5 ns in the presence of EGF. The N-terminal mRFP tag exhibited a slightly longer ϕ_{app} of 28 ± 5 ns in the absence of ligand, increasing to 58 ± 10 ns in the presence of EGF. The steady-state r measurements presented in Figure 6 demonstrate that the ϕ_{app} of the dual-tag-EGFR-ECD increases significantly in response to ligand binding (by 80 and 100% for eGFP and mRFP, respectively), indicating some sort of reduction in the level of freedom of motion of the dual-tag-EGFR-ECD when bound to EGF.

When the steady-state anisotropy of a molecule is being measured in solution, the r value (and calculated ϕ_{app}) represents an average only that depends on the size, shape, and flexibility of the labeled molecule (*25*). In the classical case of a large molecule of interest (protein) labeled with a small fluorescent probe, it is common to try to distinguish between the contribution of the local motions of the probe (ϕ_F, fast) and the global motion of the whole molecule (ϕ_S, slow) (*25*). Given the fact that no conformational or shape change was detected by FRET or AUC, and the increase in mass represents an only 5% change, we assume that the global tumbling of the dual-tag-EGFR-ECD is similar in the presence and absence of EGF. We therefore interpret the measured much larger change in ϕ_{app} upon ligand binding as a reduction in the rate or angular extent of probe motions. This could be due to either (i) a reduction in local motions of the protein itself when bound to EGF or (ii) a reduction in the local motions of the probes with respect to the protein, or both. The similar increase in correlation time experienced by both probes suggests that EGF binding transmits changes in the conformational dynamics that are experienced at both ends of the protein. This finding is in accordance with what was reported by Lammerts van Bueren et al., on reconstructed tomograms of EGFR on the cell surface (*26*). They find monomeric, resting EGFR ectodomains on the cell surface have high flexibilities, while ligand-bound EGFR complexes were found to possess little flexibility. Taken together, our data suggest that the dual-tag-EGFR-ECD undergoes a change in dynamics that accompanies ligand binding, but a much smaller change in shape compared to that predicted by a tether-to-untether (T → U) transition model.

Comparison with Other Studies. The data presented in this study suggest the dual-tag-EGFR-ECD does not undergo a T → U transition as predicted by the structural model. Rather, it appears to adopt an untethered conformation whether free or bound to EGF. Such a discrepancy between data and model could arise from two possible scenarios. In the first scenario, the T → U transition occurs but is undetected or masked by the probes attached to the EGFR-ECD. This possibility is unlikely as

two independent measurements of protein conformation indicated the same qualitative results of no conformational change upon EGF binding (AUC and lifetime based-FRET). Moreover, it is difficult to envision a T → U transition that does not change the overall shape detected by AUC and results in no detected distance change between the probes. In the second scenario, the T → U transition does not occur because the dual-tag-EGFR-ECD is in the U state due to the presence of the probes. The altered affinity for EGF, relative to the untagged receptor, suggests that this is the more likely explanation.

As described in the introductory section, there are now several studies addressing the conformation of the erbB family ectodomains in solution. Dawson et al. (*8*) identified a tethered conformation for the unliganded EGFR-ECD and an untethered one for the ligand-occupied complex using SAXS. The latter structure is consistent with the conformation of the dual-tag-EGFR-ECD−EGF complex inferred from our FRET data. Dawson et al. found it difficult to detect a ligand-free untethered conformation despite extensive mutation of tether contacts. Clearly, the addition of one or two of the probes used in our study is sufficient to elicit complete untethering in the absence of ligand. Our unliganded receptor adopts a structure that more closely resembles an untethered, extended conformation that was recently reported for the *Drosophila* EGFR-ECD analogue (*9*). Another study identified unliganded−untethered conformations of full-length EGFR on the cell surface (*26*), giving credence to the possibility that such an entity exists. The observation that insertions distal from the II−IV domain tether affect the conformational state of the EGFR-ECD suggests allosteric effects need to be considered. In their recent publication, McDonald and Pike (*27*) pointed out an important possible role of residues of the trans- and juxtamembrane domain of the EGFR in determining the conformations accessible to the EGFR-ECD. As pointed out in a recent review (*28*), there is a need to consider EGFR as a full-length allosteric enzyme. Our results seem to be in line with those notions, as having a GFP tag C-terminal to the EGFR-ECD indeed has a profound effect on the structure of the unliganded dual-tag-EGFR-ECD.

While the structure of the dual-tag-EGFR-ECD may be perturbed by the (relatively large) fluorescent proteins attached to it, the information provided with respect to the EGFR-ECD structure and function is highly valuable. This is evident upon comparison of the EGF-EGFR affinities among different ectodomain derivatives. Without the fluorescence probes at the termini, the EGFR-ECD (621 amino acids) has an affinity for EGF that is weaker by 50-fold than that of the dual-tag-EGFR-ECD. Truncation of domain IV of the EGFR-ECD (leaving 501 amino acids) increases the affinity, but relative to the dual-tag-EGFR-ECD, it is 5-fold weaker in affinity. It is apparent that extending the structure (with eGFP and mRFP) has had a stronger effect on the affinity for EGF than truncation of domain IV. Truncation presumably removes a tethered interaction and reduces the energy required to untether the receptor to form the liganded U state, but it is unclear whether the truncated receptor is tethered, untethered, or intermediate in the absence of ligand. However, in the dual-tag-EGFR-ECD, the receptor is adopting a substantially populated untethered form in the absence of ligand with the two ligand-binding domains poised for binding. Examination of the ligand-bound untethered EGFR-ECD structure (*12*) indicates that opening the receptor binding pocket to release bound ligand is less likely to occur in the untethered than in the tethered conformation which could be manifested in a slow dissociation constant (and correspondingly higher affinity) as measured here for the dual-tag-EGFR-ECD interacting with EGF in the Biacore.

Klein et al. (*29*) and others (*28*) suggested that the U form of the EGFR-ECD has a 5−20-fold higher affinity for EGF. In this work, we provide experimental support for this prediction as we measure both the high affinity and U conformation for the dual-tag-EGFR-ECD.

In conclusion, this is the first experimental report of a monomeric EGFR-ECD derivative in solution that approaches the affinity of EGFR found on the cell surface and the first evidence that an extended EGFR ectodomain has a higher affinity than a tethered one.

Studies aimed at determining the conformational states of the full-length EGFR ligand-free dimer on the cell surface are in progress and will be reported elsewhere.

SUPPORTING INFORMATION AVAILABLE

Experimental methods for cloning of the singly labeled EGFR-ECD and dual-tag-EGFR-ECD. This material is available free of charge via the Internet at http://pubs.acs.org.

REFERENCES

1. Burgess, A. W. (2008) EGFR family: Structure physiology signalling and therapeutic targets. *Growth Factors 26*, 263–274.
2. Yarden, Y., and Schlessinger, J. (1987) Self-phosphorylation of epidermal growth factor receptor: Evidence for a model of intermolecular allosteric activation. *Biochemistry 26*, 1434–1442.
3. Gadella, T. W., Jr., and Jovin, T. M. (1995) Oligomerization of epidermal growth factor receptors on A431 cells studied by time-resolved fluorescence imaging microscopy. A stereochemical model for tyrosine kinase receptor activation. *J. Cell Biol. 129*, 1543–1558.
4. Clayton, A. H., Orchard, S. G., Nice, E. C., Posner, R. G., and Burgess, A. W. (2008) Predominance of activated EGFR higher-order oligomers on the cell surface. *Growth Factors 26*, 316–324.
5. Clayton, A. H., Walker, F., Orchard, S. G., Henderson, C., Fuchs, D., Rothacker, J., Nice, E. C., and Burgess, A. W. (2005) Ligand-induced dimer-tetramer transition during the activation of the cell surface epidermal growth factor receptor-A multidimensional microscopy analysis. *J. Biol. Chem. 280*, 30392–30399.
6. Ferguson, K. M., Berger, M. B., Mendrola, J. M., Cho, H. S., Leahy, D. J., and Lemmon, M. A. (2003) EGF activates its receptor by removing interactions that autoinhibit ectodomain dimerization. *Mol. Cell 11*, 507–517.
7. Greenfield, C., Hiles, I., Waterfield, M. D., Federwisch, M., Wollmer, A., Blundell, T. L., and McDonald, N. (1989) Epidermal growth factor binding induces a conformational change in the external domain of its receptor. *EMBO J. 8*, 4115–4123.
8. Dawson, J. P., Bu, Z., and Lemmon, M. A. (2007) Ligand-induced structural transitions in ErbB receptor extracellular domains. *Structure 15*, 942–954.
9. Alvarado, D., Klein, D. E., and Lemmon, M. A. (2009) ErbB2 resembles an autoinhibited invertebrate epidermal growth factor receptor. *Nature 461*, 287–291.
10. Pham, E., Chiang, J., Li, I., Shum, W., and Truong, K. (2007) A computational tool for designing FRET protein biosensors by rigid-body sampling of their conformational space. *Structure 15*, 515–523.
11. Burgess, A. W., Cho, H. S., Eigenbrot, C., Ferguson, K. M., Garrett, T. P., Leahy, D. J., Lemmon, M. A., Sliwkowski, M. X., Ward, C. W., and Yokoyama, S. (2003) An open-and-shut case? Recent insights into the activation of EGF/ErbB receptors. *Mol. Cell 12*, 541–552.
12. Ogiso, H., Ishitani, R., Nureki, O., Fukai, S., Yamanaka, M., Kim, J. H., Saito, K., Sakamoto, A., Inoue, M., Shirouzu, M., and Yokoyama, S. (2002) Crystal structure of the complex of human epidermal growth factor and receptor extracellular domains. *Cell 110*, 775–787.
13. Luwor, R. B., Johns, T. G., Murone, C., Huang, H. J., Cavenee, W. K., Ritter, G., Old, L. J., Burgess, A. W., and Scott, A. M. (2001) Monoclonal antibody 806 inhibits the growth of tumor xenografts expressing either the de2-7 or amplified epidermal growth factor receptor (EGFR) but not wild-type EGFR. *Cancer Res. 61*, 5355–5361.
14. Gill, S. C., and von Hippel, P. H. (1989) Calculation of protein extinction coefficients from amino acid sequence data. *Anal. Biochem. 182*, 319–326.

15. Schuck, P. (2000) Size-distribution analysis of macromolecules by sedimentation velocity ultracentrifugation and Lamm equation modeling. *Biophys. J. 78*, 1606–1619.
16. Harding, S. E., Horton, J. C., and Rowe, A. J. (1992) Computer-aided interpretation of analytical sedimentation data for proteins. In Analytical Ultracentrifugation in Biochemistry and Polymer Science, pp 90−125, Royal Society of Chemistry, London.
17. Clayton, A. H., Tavarnesi, M. L., and Johns, T. G. (2007) Unligated epidermal growth factor receptor forms higher order oligomers within microclusters on A431 cells that are sensitive to tyrosine kinase inhibitor binding. *Biochemistry 46*, 4589–4597.
18. Domagala, T., Konstantopoulos, N., Smyth, F., Jorissen, R. N., Fabri, L., Geleick, D., Lax, I., Schlessinger, J., Sawyer, W., Howlett, G. J., Burgess, A. W., and Nice, E. C. (2000) Stoichiometry, kinetic and binding analysis of the interaction between epidermal growth factor (EGF) and the extracellular domain of the EGF receptor. *Growth Factors 18*, 11–29.
19. Elleman, T. C., Domagala, T., McKern, N. M., Nerrie, M., Lonnqvist, B., Adams, T. E., Lewis, J., Lovrecz, G. O., Hoyne, P. A., Richards, K. M., Howlett, G. J., Rothacker, J., Jorissen, R. N., Lou, M., Garrett, T. P., Burgess, A. W., Nice, E. C., and Ward, C. W. (2001) Identification of a determinant of epidermal growth factor receptor ligand-binding specificity using a truncated, high-affinity form of the ectodomain. *Biochemistry 40*, 8930–8939.
20. Jorissen, R. N., Walker, F., Pouliot, N., Garrett, T. P. J., Ward, C. W., and Burgess, A. W. (2003) Epidermal growth factor receptor: Mechanisms of activation and signalling. *Exp. Cell Res. 284*, 31–53.
21. Liu, P., Sudhaharan, T., Koh, R. M., Hwang, L. C., Ahmed, S., Maruyama, I. N., and Wohland, T. (2007) Investigation of the dimerization of proteins from the epidermal growth factor receptor family by single wavelength fluorescence cross-correlation spectroscopy. *Biophys. J. 93*, 684–698.
22. Burgess, B. R., Dobson, R. C., Bailey, M. F., Atkinson, S. C., Griffin, M. D., Jameson, G. B., Parker, M. W., Gerrard, J. A., and Perugini, M. A. (2008) Structure and evolution of a novel dimeric enzyme from a clinically important bacterial pathogen. *J. Biol. Chem. 283*, 27598–27603.
23. Peter, M., Ameer-Beg, S. M., Hughes, M. K., Keppler, M. D., Prag, S., Marsh, M., Vojnovic, B., and Ng, T. (2005) Multiphoton-FLIM quantification of the EGFP-mRFP1 FRET pair for localization of membrane receptor-kinase interactions. *Biophys. J. 88*, 1224–1237.
24. Hink, M. A., Griep, R. A., Borst, J. W., van Hoek, A., Eppink, M. H., Schots, A., and Visser, A. J. (2000) Structural dynamics of green fluorescent protein alone and fused with a single chain Fv protein. *J. Biol. Chem. 275*, 17556–17560.
25. Lakowicz, J. R. (1999) Principles of fluorescence spectroscopy, 2nd ed., Kluwer Academic/Plenum Publishers, Dordrecht, The Netherlands.
26. Lammerts van Bueren, J. J., Bleeker, W. K., Brannstrom, A., von Euler, A., Jansson, M., Peipp, M., Schneider-Merck, T., Valerius, T., van de Winkel, J. G., and Parren, P. W. (2008) The antibody zalutumumab inhibits epidermal growth factor receptor signaling by limiting intra- and intermolecular flexibility. *Proc. Natl. Acad. Sci. U.S.A. 105*, 6109–6114.
27. Macdonald-Obermann, J. L., and Pike, L. J. (2009) The intracellular juxtamembrane domain of the epidermal growth factor (EGF) receptor is responsible for the allosteric regulation of EGF binding. *J. Biol. Chem. 284*, 13570–13576.
28. Lemmon, M. A. (2009) Ligand-induced ErbB receptor dimerization. *Exp. Cell Res. 315*, 638–648.
29. Klein, P., Mattoon, D., Lemmon, M. A., and Schlessinger, J. (2004) A structure-based model for ligand binding and dimerization of EGF receptors. *Proc. Natl. Acad. Sci. U.S.A. 101*, 929–934.